Table IV. Coefficients in the HOMO's of the CH_5^- and SiH_5^- Complexes with the Core Atomic Orbitals Omitted

	CH_5^-		SiH_5^-	
	6-31G+D	6-31G*+D	6-31G+D	6-31G*+D
central atom				
inner s	0.1418	0.1347	−0.0362	−0.0010
outer s	0.0417	0.0700	0.2094	0.0383
d		0.0444		0.1619
equatorial H				
inner s	0.0659	0.0581	0.1320	0.1717
outer s	0.1732	0.1616	0.2858	0.2561
axial H				
inner s	−0.2052	−0.2087	−0.2101	−0.2075
outer s	−0.4072	−0.4029	−0.5386	−0.4439
diffuse s	−0.2945	−0.2890	−0.0877	−0.1022

accessible for mixing than $\sigma^*(CH_3)$. As a result the HOMO of SiH_5^- should contain more $\sigma^*(MH_3)$ character than the HOMO of CH_5^-. It is expected accordingly that in comparison with HOMO(CH_5^-), HOMO(SiH_5^-) will involve smaller coefficients on the central atom and larger coefficients on the equatorial hydrogens. The calculated orbitals in Table IV show the latter effect but are not clear for the former. The total effect of $\sigma^*(MH_3)$ mixing is certainly spread over the two a'_1 orbitals of MH_5^-, and it is therefore not easy to reconstruct an argument based on one orbital alone.

There should be no contest between MO and VB; one should be preferred over the other depending on the insight they provide in each specific problem. We think that, in the present problem, the VB treatment in terms of the avoided-crossing diagrams (Figures 3-5) provides insight into the relative stability of SiH_5^- and CH_5^- in a manner that is vivid and instructive. Moreover, on the basis of the bonding descriptions of these species in **9-11**, it is apparent that the qualitative Si-C difference should highly depend on electron count. Thus, removal of one electron will generate the 9-electron species $SiH_5^\bullet$ and $CH_5^\bullet$, which according to **9-11** should both involve a single bond pair of the p-type and behave qualitatively the same. Indeed, both $SiH_5^\bullet$ and $CH_5^\bullet$ are *transition states* along the $H_l + MH_3H_r \rightarrow H_lMH_3 + H_r$ reaction coordinate.[33] It is not easy to come up with a straightforward MO explanation (e.g. based on the HOMOs) of this change upon removal of one electron from the system.

(33) Maitre, P.; Pelissier, M.; Volatron, F. 6-31G*-MP2//6-31G*-MP2 results, manuscript in preparation.

Summary

The qualitative difference between CH_5^- and SiH_5^- is studied by VB computations of avoided-crossing diagrams.[11-19] The diagrams reveal that the stability and compact geometry of SiH_5^- (percentagewise relative to SiH_4) originate in a VB configuration which falls (Figures 4 and 5) below the two classical Lewis structures. This VB configuration involves two axial Si-H_{ax} bonds: one utilizes silicon's axial p-AO and the other utilizes the $\sigma^*(SiH_3)$ orbital. Thus, SiH_5^- lowers its energy relative to its parent fragments (H^-/SiH_4) by delocalizing the fifth valence electron pair into the equatorial Si-H bonds.

In the case of CH_5^-, the diagram (Figure 3) shows that the bonding primarily arises from the avoided crossing of two classical Lewis structures. This produces a high-energy transition state, which possesses a resonating single four-electron/three-center H_{ax}--C--H_{ax} bond. The axial linkages are therefore long relative to the equatorial bonds, and the fifth valence electron pair is localized in the axial portion of the trigonal-bipyramidal structure.

The difference between SiH_5^- and CH_5^- is related to the electropositivity of Si relative to C. This factor endows the $\sigma^*(SiH_3)$ orbital with a bonding capability: low p $\rightarrow \sigma^*$ promotion energy and ability to sustain a high overlap with H_{ax}. This same factor deprives $\sigma^*(CH_3)$ from such capability. Clark[34] has invoked similar overlap arguments to explain the stability of the 9-valence-electron SiH_3Cl^- species, relative to the dissociative behavior of the analogous CH_3Cl^- species. Arguments of another type have been used by Gronert, Glaser, and Streitwieser[35] to explain the stability of SiH_4F^-. Using integrated projection populations, these authors find the silicon atom to have considerable ionic character in this complex and conclude that its stability arises from ionic contributions. We do not think, however, that such an explanation can be extended to the SiH_5^- case, since the ionic contributions are included, within our calculation, in the Lewis structures **1** and **2**, which yield a barrier and not a stable intermediate.

Registry No. SiH_5^-, 41650-16-2; CH_5^-, 12316-54-0.

(34) Clark, T. *J. Chem. Soc., Chem. Commun.* **1981**, 515.
(35) Gronert, S.; Glaser, R.; Streitwieser, A. *J. Am. Chem. Soc.* **1989**, *111*, 3111.

Investigation by MCD of the Low-Lying Electronically Excited States of Some Selected Quinoid Diones

J. Frei, H. Yamaguchi,† J. Tsunetsugu,‡ and G. Wagniere*

Contribution from the Institute of Physical Chemistry, Winterthurerstrasse 190, CH-8057 Zurich, Switzerland. *Received September 16, 1988*

Abstract: The MCD spectra of some quinoid dicarbonyl compounds of pseudoaromatic or antiaromatic character have been recorded. These spectra, combined with calculations of the *B*-terms by the PPP method, provide a detailed analysis of the long wavelength $\pi\pi^*$ bands. Some transitions show a marked charge-transfer character. In one compound we believe to have identified the *A*-term of the $S_0 \rightarrow T_1(^3\pi\pi^*)$ transition.

1. Introduction

In a previous investigation,[1] hereafter designated as I, the long wavelength MCD spectra of some simple *o*- and *p*-quinones have been examined. It has been shown that the signals due to the lower $\pi\pi^*$ transitions in the near-UV may be well-interpreted by the PPP model. The spectra in conjunction with calculations, give information on the polarization of the corresponding bands. The much weaker MCD signals due to the $n\pi^*$ transitions were identified with the help of CNDO calculations. A very weak long wavelength *A*-term appearing in the spectra of some of the com-

* Author to whom correspondence should be addressed.
† Permanent address: Ibaraki University, College of Technology, 4-12-1 Nakanarusawa, Hitachi 316, Japan.
‡ Permanent address: Department of Chemistry, Faculty of Science, Saitama University, Urawa, Saitama 338, Japan.

(1) Meier, A. R.; Wagnière, G. H. *Chem. Phys.* **1987**, *113*, 287.

0002-7863/90/1512-1413$02.50/0

pounds was assigned to the $S_0 \rightarrow T_1(^3n\pi^*)$ absorption. The noted difference between the spectra of *o*- and *p*-quinones was emphasized.

In the present report we consider the spectra of some compounds which all contain a 1,4-dione moiety fused to an antiaromatic or pseudoaromatic hydrocarbon chromophore. As we shall see, this situation leads to both localized as well as to charge-transfer transitions. The study of such aspects is one of our aims. In simple *p*-quinones the $n\pi^*$ transitions occur at relatively short wavelengths and are almost degenerate. In the compounds studied here, calculations of the energy of the $n\pi^*$ states predict an analogous situation. It must be assumed that both in absorption and in MCD the corresponding very weak signals are not, or only barely, detectable under the much stronger contributions of the $\pi\pi^*$ bands. We therefore focus our attention mainly on the $\pi\pi^*$ transitions.

2. Experimental Section

The MCD spectra were measured and recorded with equipment under conditions described in I. For practical reasons the measurements reported here were carried out at room temperature with an Oxford Instruments SM-1 cryomagnet at 5.0 T, instead of the SM-4 cryomagnet at 5.26 T used previously.[2]

Compound **1** was prepared as reported.[3] Compound **2** was synthesized by Prof. M. Oda of Osaka University. Compounds **3** and **4** were synthesized by one of the authors (J.T.).[4-6] All compounds were recrystallized three times from cyclohexane.

The emission spectrum of compound **2** was measured on a SPEX Fluorolog with DM1B data processor.

3. Calculations

A summary of the theory of MCD is given in the Appendix of I, and further details are to be found in ref 7-12. The calculation of the *B*-terms was based on an SCF-MO single-CI procedure in the frame of the PPP approximation.[13] The CNDO method was used to assess the energy of the $n\pi^*$ states. Information concerning the parametrization of the semiempirical calculations may be inferred from I. In the absence of relevant experimental structural data, the geometry of molecules **1-4** was optimized by using the MNDO method.[14] The relation between the theoretical quantity *B* and the measured quantity $[\theta]_M$ is given by the relation[15]

$$B = -(1/33.53) \int_{\text{band}} \frac{[\theta]_M}{\nu} \, d\nu$$

It is only applicable where bands arising from different electronic transitions do not overlap too strongly.

4. Results and Discussion

The measured and calculated spectra are shown in Figures 1-4. A general discussion of the results follows.

(a) Compound 1 [2-(2,4,6-Cycloheptatrien-1-ylidene)-4-cyclopentene-1,3-dione]. Figure 1 (top) shows that the strongest (negative) long wavelength MCD signal around 450 nm does not coincide with the absorption maximum at about 400 nm, in contrast to what one would expect. The calculation predicts the long wavelength $\pi\pi^*$ transitions to occur at somewhat shorter wavelengths, as compared to the experiment. It is seen that the broad absorption band should involve three electronic $\pi\pi^*$ transitions of polarization *z*,*z*,*y* to the excited states numbered, respectively, 1, 2, and 3 (see Table I). From the calculation one obtains by far the largest *f*-value (~0.32) for the *y*-polarized transition $G \rightarrow 3$, but, on the other hand, the biggest (positive) *B*-term for the very weak *z*-polarized transition $G \rightarrow 2$. For this reason it is instructive to analyze the main contributions which

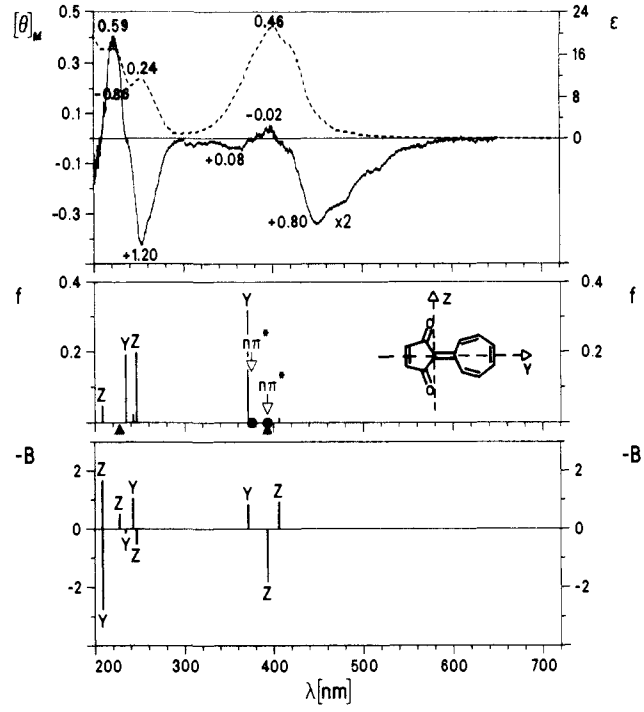

Figure 1. Data on compound **1**. Top: Absorption spectrum (dashed). MCD spectrum (solid line) in the region above 300 nm magnified ×2 with respect to the $[\theta]_M$ scale at left: solvent, cyclohexane; ϵ in units 10^3·L mol^{-1} cm^{-1}; $[\theta]_M$ in deg cm^2 dmol^{-1} G^{-1}. Experimental *f* values, and *B* values in units 10^{-3}·$D^2\mu_B$ cm deduced by graphical integration. Middle: Calculated *f* values and polarization of the $\pi\pi^*$ transitions. Calculated position of the $n\pi^*$ transitions. Very weak $\pi\pi^*$ transitions are indicated by triangles below the wavelength scale. Bottom: Calculated polarizations and negative *B* values of the $\pi\pi^*$ transitions in 10^{-3}·$D^2\mu_B$ cm (see also I).

Table I. Calculated Data on Ground (G) and Lower Excited States of Compounds **1-4**[a]

compd	state	calcd energy (eV)	main configuration	c^2	calcd state dipole moment (*D*)
1	*G*				3.44
	1 *z*	3.05	7 → 9*	0.82	13.77
	2 *z*	3.15	7 → 10*	0.88	-4.05
	3 *y*	3.34	7 → 8*	0.94	5.35
2	*G*				2.69
	1 *z*	1.79	7 → 8*	0.99	2.81
	2 *y*	3.03	7 → 9*	0.97	14.69
	3 *y*	4.67	6 → 8*	0.95	-11.39
3	*G*				2.65
	1 *z*	2.91	9 → 10*	0.80	9.52
	2 *z*	3.49	7 → 10*	0.68	5.89
	3 *y*	3.52	8 → 10*	0.96	6.34
4	*G*				1.08
	1 *z*	2.97	11 → 12*	0.79	7.03
	2 *z*	3.55	9 → 12*	0.61	3.63
	3 *y*	3.58	10 → 12*	0.93	2.91

[a] The configuration mainly involved in a given excited state is indicated in terms of the excitation between SCF MO's (see Figures 5, 6, 10, and 11). The coefficient *c* squared gives the corresponding fractional contribution. Notice the reversal of the sign of the dipole moment of excited state 2 in compound **1** and of excited state 3 in compound **2**.

(2) Meier, A. R. Doctoral Thesis, University of Zurich, Switzerland, 1986.
(3) Kitahara, Y.; Murata, I.; Asano, T. *Bull. Chem. Soc. Jpn.* **1961**, *34*, 589.
(4) Tsunetsugu, J.; Ikeda, T.; Suzuki, N.; Yaguchi, M.; Sato, M.; Ebine, S.; Morinaga, K. *J. Chem. Soc., Perkin Trans. 1* **1985**, 785.
(5) Tsunetsugu, J.; Ikeda, T.; Suzuki, N.; Yaguchi, M.; Sato, M.; Ebine, S.; Morinaga, K. *J. Chem. Soc., Chem. Commun.* **1983**, 28.
(6) Lown, J. W.; Aidoo, A. S. K. *Can. J. Chem.* **1971**, *49*, 1861.
(7) Buckingham, A. D.; Stephens, P. J. *Ann. Rev. Phys. Chem.* **1966**, *17*, 399.
(8) Schatz, P. N.; McCaffery, A. J.; Suëtaka, W.; Henning, G. N.; Ritchie, A. B.; Stephens, P. J. *J. Chem. Phys.* **1966**, *45*, 722.
(9) Seamans, L.; Moscowitz, A. *J. Chem. Phys.* **1972**, *56*, 1099.
(10) Warnick, S. M.; Michl, J. *J. Am. Chem. Soc.* **1974**, *96*, 6280.
(11) Obbink, J. H.; Hezemans, A. M. F. *Theor. Chim. Acta* **1976**, *43*, 75.
(12) Michl, J. *J. Am. Chem. Soc.* **1978**, *100*, 6801. Jonas, I.; Michl, J. *J. Am. Chem. Soc.* **1978**, *100*, 6834. Otteson, D.; Michl, J. *J. Am. Chem. Soc.* **1978**, *100*, 6857.
(13) *B*-term program by A. R. Meier, University of Zurich. A FORTRAN listing may be obtained from one of the authors (G.W.) upon written request. See I for further references.
(14) Dewar, M. J. S.; Zoebisch, E. G.; Healy, E. F.; Stewart, J. J. P. *J. Am. Chem. Soc.* **1985**, *107*, 3902.
(15) Stephens, P. J. *Chem. Phys. Lett.* **1968**, *2*, 241.

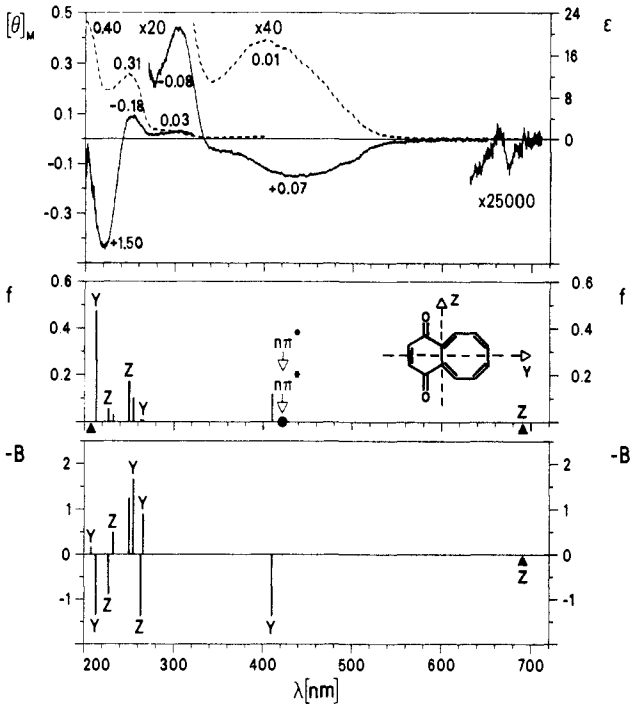

Figure 2. Data on compound **2**. Top: Absorption spectrum (dashed), MCD spectrum (solid line) in cyclohexane. Experimental f and B values. In the 300–700-nm range the absorption spectrum is magnified ×40, the MCD spectrum ×20. Notice the very weak MCD signal at 670 nm measured in benzene, magnified $\times 2.5\times 10^4$. Middle: Calculated f values and polarizations of the $\pi\pi^*$ transitions. Very weak transitions are indicated by triangles. Calculated position of the $n\pi^*$ transitions. Bottom: Calculated ($-B$) values for the $\pi\pi^*$ transitions.

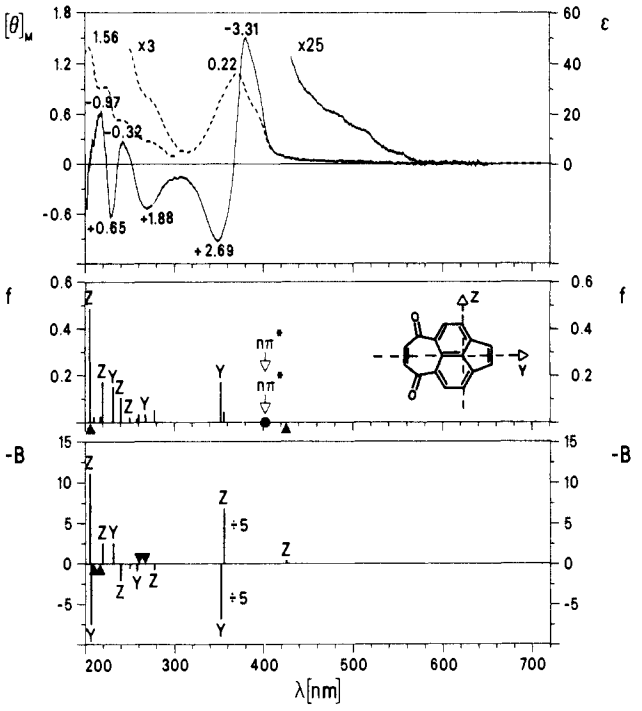

Figure 3. Data on compound **3**. Top: Absorption spectrum (dashed), MCD spectrum (solid line) in cyclohexane. Experimental f and B values. In the 260–710-nm range the absorption spectrum is magnified ×3. Beyond 430 nm the tail of the MCD spectrum is magnified ×25. Middle: Calculated f values and polarizations of the $\pi\pi^*$ transitions. Calculated position of the (almost degenerate) $n\pi^*$ transitions. Bottom: Calculated ($-B$) values for the $\pi\pi^*$ transitions. The length of the bars for the two close-lying, y-respectively z-polarized, transitions with opposite sign just below 360 nm are reduced by a factor of 5 with respect to the calculated values.

enter the calculation of the B-terms (see expression A.2c in I) of these long wavelength transitions. The sums over states were truncated after the tenth excited state.

The most important contribution to $B(G \rightarrow 1)$, the (negative) B-term of the transition $G \rightarrow 1$, is

$$(E_3 - E_1)^{-1}\mathrm{Im}(\langle 1|\vec{m}|3\rangle \cdot \langle G|\vec{\mu}|1\rangle \times \langle 3|\vec{\mu}|G\rangle) \qquad (1)$$

The electric dipole transition moment $\langle 3|\vec{\mu}|G\rangle$ is large, $\langle G|\vec{\mu}|1\rangle$ is much smaller. The magnetic dipole transition moment $\langle 1|\vec{m}|3\rangle$ arises, on the one-electron level, mainly from the corresponding matrix element between (virtual) SCF MO's 8* and 9* (see Table I and Figure 5). It involves predominantly AO's on the carbon atoms of the five-membered ring and on the two oxygen atoms. One reason why the expected relatively weak positive long wavelength MCD signal is not observed in the experiment may be that the PPP model exaggerates the magnitude of this relatively localized magnetic dipole transition moment.

The term making the biggest and dominant contribution to the summation for $B(G \rightarrow 2)$ is identified as

$$(E_3 - E_2)^{-1}\mathrm{Im}(\langle 2|\vec{m}|3\rangle \cdot \langle G|\vec{\mu}|2\rangle \times \langle 3|\vec{\mu}|G\rangle) \qquad (2)$$

It is opposite in sign to (1). The relatively large magnetic transition moment $\langle 2|\vec{m}|3\rangle$ arises at the one-electron level predominantly from the matrix element between SCF MO's 8* and 10*. It involves mainly AO's on the carbon atoms of the seven-membered ring. The term $B(G \rightarrow 2)$ undoubtedly gives rise to the dominant broad negative MCD maximum in the 450-nm region. It then seems likely that the weak positive MCD signal at 400 nm is due to $B(G \rightarrow 3)$. This latter B-term contains a superposition of contributions of the kind given by expressions 1 and 2. These contributions enter with opposite signs.

In summary, we may conclude that the absorption maximum at 400 nm is due to a y-polarized transition, whereas the negative MCD maximum at 450 nm arises from a weak z-polarized component within the long wavelength tail of the broad 350–450-nm band. The magnitude of this MCD signal mainly stems from the magnetic dipole transition moment between excited $\pi\pi^*$ states 2 and 3 of respective symmetry B_1 and A_1 under C_{2v}. The contributions to the MCD of the close-lying $n\pi^*$ excited states have not been taken into account in our calculations. From our observations in I and from symmetry considerations, we have reason to believe that these contributions are relatively small.

The two large MCD signals of opposite sign between 200 and 300 nm appear to be simple in structure. The PPP model, however, predicts such a large number of excited states in this region that a clear-cut interpretation of the shorter wavelength MCD bands does not seem possible.

Returning to the calculations on the lower excited states (Table I), we notice the rather unusual fact that the dipole moment of state 1 is very large but parallel to that of the ground state, while that of state 2 though smaller has opposite sign. Indeed, the one-electron transition 7 → 9* shows a transfer of charge to the dione moiety, while the transition 7 → 10* involves a transfer to the seven-membered ring (Figure 5).

(b) Compound 2 [1,4-Benzocyclooctenedione] (Figure 2). The calculation predicts a very weak z-polarized transition, $G \rightarrow 1$, at 691 nm, followed only at 410 nm by the stronger y-polarized transition, $G \rightarrow 2$. A cursory examination of the spectra gives the fallacious impression that $G \rightarrow 1$ is not detectable. We shall return to this point subsequently. On the basis of the calculation, the broad, relatively weak band between 350 and 500 nm should, aside from possible weaker $n\pi^*$ contributions, be mainly due to the single $\pi\pi^*$ transition $G \rightarrow 2$. The sums leading to $B(G \rightarrow 2)$ were truncated after 15 excited states. By far the most important term in the summations reads

$$(E_1 - E_0)^{-1}\mathrm{Im}(\langle 1|\vec{m}|G\rangle \cdot \langle G|\vec{\mu}|2\rangle \times \langle 2|\vec{\mu}|1\rangle) \qquad (3)$$

Interestingly, the transition $G \rightarrow 1$ is quite strongly magnetic dipole allowed. On the one-electron level this implies that the matrix element (see Table I and Figure 6) $\langle 7|\vec{m}|8^*\rangle$ should be large. We notice that both SCF MO's 7 and 8* are strongly localized on the eight-membered ring. The vector $\langle 7|\vec{m}|8^*\rangle$ lies in the x-direction, perpendicular to the molecular plane. Although the

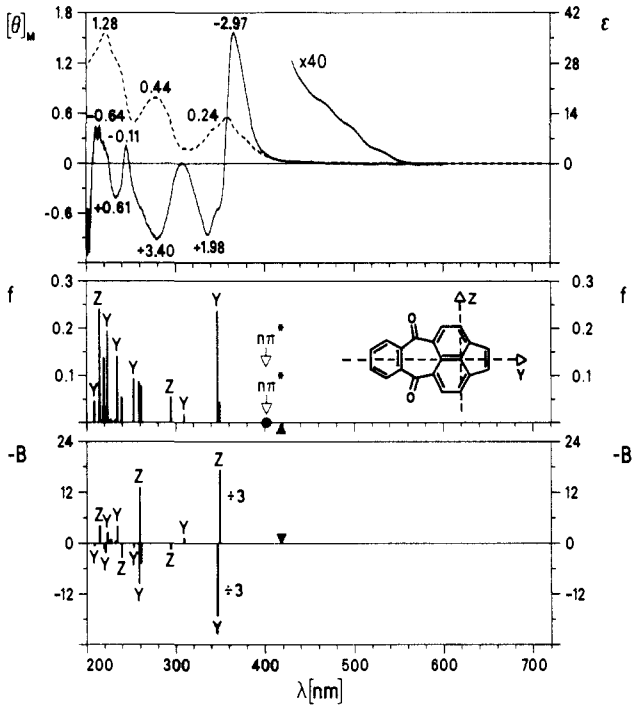

Figure 4. Data on compound **4**. Top: Absorption spectrum (dashed), MCD spectrum (solid line) in cyclohexane. Experimental f and B values. Beyond 430 nm the tail of the MCD spectrum is magnified ×40. Middle: Calculated f values and polarization of the $\pi\pi^*$ transitions. Calculated position of the $n\pi^*$ transitions. Bottom: Calculated ($-B$) values for the $\pi\pi^*$ transitions. The length of the bars for the two close-lying, y-respectively z-polarized, transitions with opposite sign near 350 nm are reduced by a factor of 3 with respect to the calculated values.

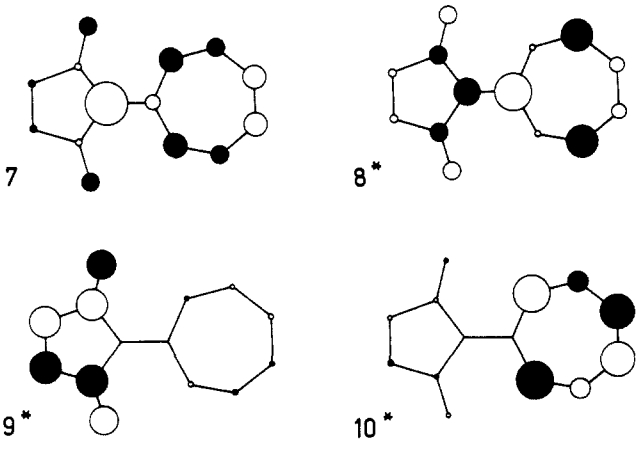

Figure 5. Highest occupied (7) and lowest unoccupied (8*, 9*, 10*) PPP SCF MO's for compound **1**. The radii of the circles are proportional to the respective LCAO coefficients. The shading indicates the relative signs. Notice the pronounced localization on the dione moiety in 9* and on the seven-membered ring in 10*.

MNDO calculation predicts a slight deviation of the eight-membered ring from planarity, we have based our PPP calculations on a planar structure. The electric dipole transition moment between excited states 1 and 2, $\langle 2|\vec{\mu}|1\rangle$, stems mainly from the one-electron matrix element between MO's 9* and 8*, $\langle 9^*|\vec{\mu}|8^*\rangle$. The transition shows a pronounced charge-transfer character. The dipole moments of the states G, 1, 2 themselves, however, do not directly affect $B(G \rightarrow 2)$. This is due to the fact that the transition moment $\langle G|\vec{\mu}|2\rangle$ is colinear with the dipole moments.

As is the case for compound **1**, the MCD signals of **2** at 300 nm and below are difficult to interpret on account of the high density of states. Notice the reversal of the sign of the large dipole moment of state 3 (Table I).

We now return to the examination of $G \rightarrow 1$. Careful 32-fold slow scanning of the MCD over the range 630–710 nm reveals

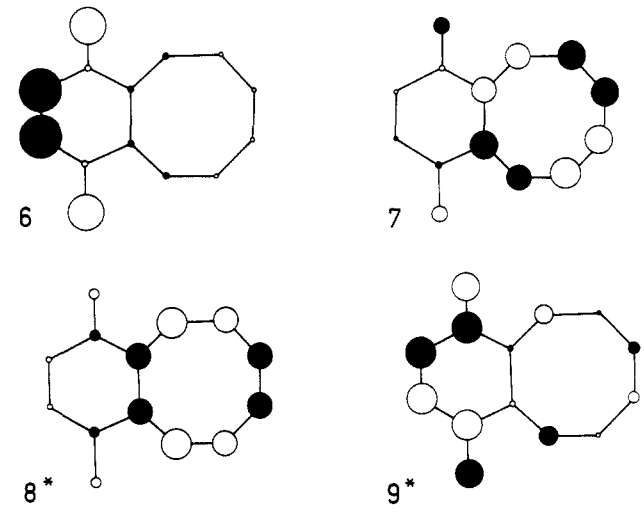

Figure 6. Highest occupied (6, 7) and lowest unoccupied (8*, 9*) MO's for compound **2**. Notice the strong localization on the dione moiety in 6 and 9* and on the eight-membered ring in 7 and 8*.

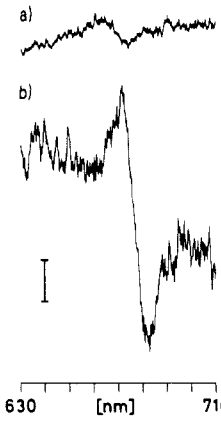

Figure 7. Long wavelength MCD signal of compound **2** in (a) benzene and (b) iodobenzene. The vertical bar at left corresponds to 10^{-5} deg cm^2 dmol^{-1} G^{-1}.

after averaging a very weak double-signed signal at about 670 nm which appears as an A-term. To ascertain that this is not an artifact, the measurements were repeated several times under varying conditions of measurement. By using iodobenzene instead of benzene as a solvent, the signal was clearly enhanced (Figure 7). Furthermore, similar long wavelength scans were carried out with the other compounds **1**, **3**, and **4** but turned out to be negative. In view of the relatively high noise level from which it was extracted, we identify with caution this signal in **2** as a true A-term. We conclude that such a signal can only arise from the $^1G \rightarrow {}^3$1 ($^3\pi\pi^*$) transition.

The question arises why one should detect the A-term for the transition $^1G \rightarrow {}^3$1 but not the B-term for $^1G \rightarrow {}^1$1. The calculated absolute value for $B(^1G \rightarrow {}^1$1) is indeed less than 10^{-2} times that for $B(^1G \rightarrow {}^1$2). If furthermore this signal is broadened by unresolved vibronic interaction, its detection should become difficult. On the other hand, the A-term, albeit very weak, has a characteristic double-signed shape. But in order for the $^1G \rightarrow {}^3$1 transition to show up in the MCD, it must borrow intensity from at least two differently polarized electric dipole-allowed singlet–singlet transitions (see I). A possibility is that spin-orbit interaction couples the ^{3}1($^3\pi\pi^*$) state to the ^{1}2($^1\pi\pi^*$) state (the transition to ^1G is y-polarized) and concomitantly to one of the $^1n\pi^*$ states (the transition calculated by CNDO to ^1G is x-polarized but weak).

In order to clarify the situation from the experimental point of view, we have measured the emission spectrum of **2** (Figure 8). One notices a long wavelength tail with vibronic structure extending beyond 800 nm. Our attempt to detect phosphorescence in the region beyond 670 nm, by looking at emission with a delay time $\tau \geq 20$ μs, has not been successful, however. Assuming that

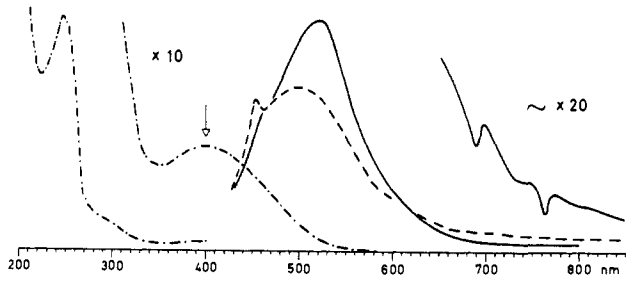

Figure 8. Long wavelength absorption (·—·), emission at room temperature (– –), and emission at 80 K (—) of compound **2** on a relative scale. All spectra in EPA solvent. The excitation wavelength for the emission spectra was 400 nm (arrow).

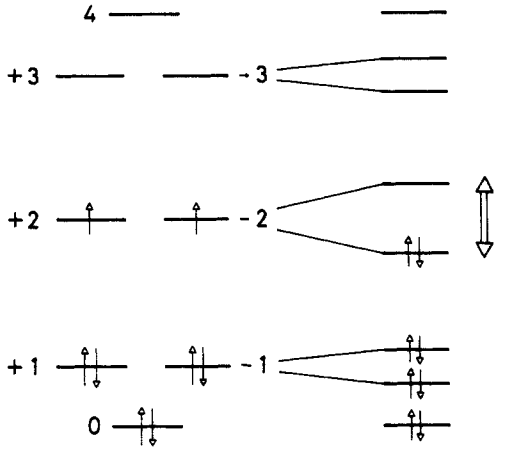

Figure 9. Energy level diagram and electron occupation in the ground configuration of the cyclic eight-membered π-electron system. Left: Perfect 8-fold symmetry. Right: Qualitative splitting of degenerate levels due to symmetry reduction. The arrow at right indicates the transition related to the weak long wavelength absorption in compound **2**.

the low-energy S_1 state is calculated correctly, it appears that the main fluorescence comes from the S_2 state, which must be due to the unusually large S_1–S_2 energy gap.

The symmetry properties of the long wavelength $G \rightarrow 1$ transition may be understood on the basis of the π electron model of the perfect eight-membered cyclic polyene (Figure 9). From the orbital picture in Figure 6, we recognize that the SCF MO's 7 and 8*, which are mainly involved, are related to the linear combinations of symmetry orbitals:

$$\varphi_+ = 1/\sqrt{2}(|+2\rangle + |-2\rangle) \quad \text{and}$$

$$\varphi_- = 1/i\sqrt{2}(|+2\rangle - |-2\rangle) \quad (4)$$

The matrix element $\langle\varphi_+|\vec{\mu}|\varphi_-\rangle$ is strictly zero, while $\langle\varphi_+|\vec{m}|\varphi_-\rangle$ is nonzero. The breakdown of cyclic symmetry lifts the degeneracy of $|+2\rangle$ and $|-2\rangle$, thereby giving a very weak electric dipole allowed increment to $7 \rightarrow 8^*$, i.e., to $G \rightarrow 1$, as indicated in Figure 9 on the righthand side by a double arrow.

(c) Compounds 3 and 4 [Cyclohept[*fg*]acenaphthylene-5,8-dione and Cyclohepta[*cd*]pleiadene-5,10-dione] (Figures 3 and 4). We notice the analogy between both compounds in the long wavelength part of the spectra. The very weak z-polarized $\pi\pi^*$ transition $G \rightarrow 1$, predicted to occur at a wavelength above 400 nm as well as the close-lying $n\pi^*$ transitions are apparently responsible for the tail of the MCD spectrum. A dominant contribution to the transition $G \rightarrow 1$ seems to be the excitation between SCF MO's 9 and 10* in compound **3** and between MO's 11 and 12* in compound **4**. This HOMO–LUMO excitation has a pronounced charge-transfer character (Table I and Figures 10 and 11), as is also borne out in the calculation by the large dipole moment of the first excited state.

Both compounds show in the 300–400-nm region a strong characteristic double-signed MCD signal. The calculation predicts that the 350-nm absorption band consists of two electronic

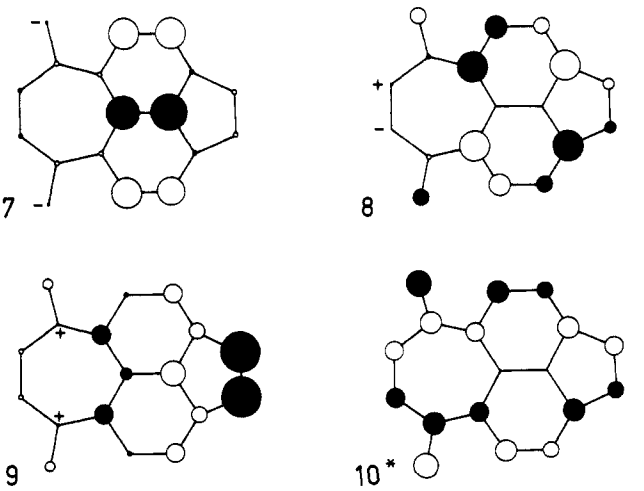

Figure 10. Highest occupied (7, 8, 9) and lowest unoccupied (10*) MO's for compound **3**. Where the coefficients are very small, only the corresponding signs (black = plus) are indicated.

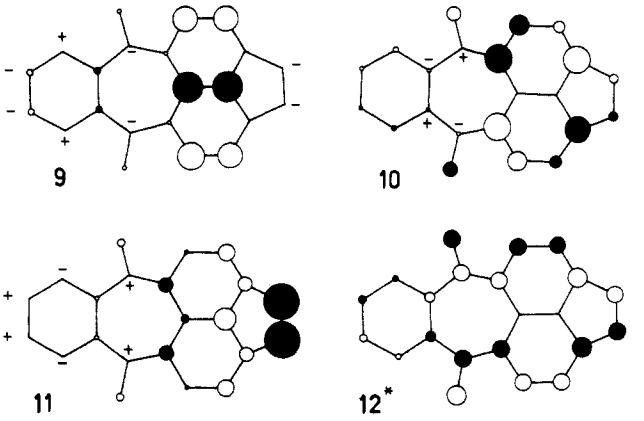

Figure 11. Highest occupied (9, 10, 11) and lowest unoccupied (12*) MO's for compound **4**. Compare with Figure 10. Notice the small participation of the AO's on the isolated six-membered ring.

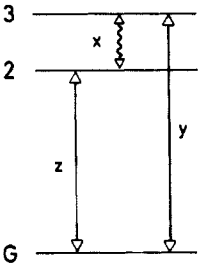

Figure 12. Qualitative energy level scheme showing as arrows the z- and y-polarized electric transition moments (straight lines) and the x-polarized magnetic transition moment (wavy line) giving rise to the pronounced pseudo-A-term which occurs in the 300–400-nm region of compounds **3** and **4**.

transitions, a weaker z-polarized one, $G \rightarrow 2$, immediately followed by a stronger y-polarized one, $G \rightarrow 3$. Examination of the B-terms shows the following major contribution:

$$B(G \rightarrow 2) \approx (E_3 - E_2)^{-1} Im(\langle 2|\vec{m}|3\rangle \cdot \langle G|\vec{\mu}|2\rangle \times \langle 3|\vec{\mu}|G\rangle) \quad (5a)$$

and

$$B(G \rightarrow 3) \approx (E_2 - E_3)^{-1} Im(\langle 3|\vec{m}|2\rangle \cdot \langle G|\vec{\mu}|3\rangle \times \langle 2|\vec{\mu}|G\rangle) \quad (5b)$$

thus

$$B(G \rightarrow 2) \approx -B(G \rightarrow 3) \quad (5c)$$

This is the situation typical of a pseudo-A-term, as defined in I. Of importance are the close energetic proximity of the excited states 2 and 3 as well as the large x-polarized magnetic transition moment between them (see Figure 12). This magnetic transition moment $\langle 2|\vec{m}|3\rangle$ involves mainly the SCF MO's 7 and 8 in

compound **3** and the MO's 9 and 10 in compound **4** (Table I, Figures 10 and 11). We notice a high involvement of the AO's on the two fused six-membered rings. In compound **4**, the isolated six-membered ring on the other side of the dione moiety participates very little in the transitions at wavelengths above 300 nm. Below 300 nm a detailed interpretation of the MCD spectra on the basis of calculations becomes difficult. One notices, however, that a remarkable analogy between **3** and **4** in the sequence of the signs persists.

The possibility that in compounds **3** and **4** the transition $G \rightarrow 2$ ($S_0 \rightarrow S_2$) be y-polarized and the transition $G \rightarrow 3$ ($S_0 \rightarrow S_3$) be z-polarized is also compatible with the observed MCD. Since the calculated transitions are very close in energy, an independent experimental determination of the absolute polarization of these transitions might here be particularly helpful. Following the suggestion of one of the referees, we have performed linear dichroism measurements of compounds **1–4** in stretched foils;[16] we have used both polyethylene and poly(vinylalcohol). The results have been inconclusive. In the polyethylene foils we were not able to obtain a sufficient concentration of the compounds, probably due to their polarity. In poly(vinylalcohol) the orientation by stretching proved to be very small, possibly due to the fact that the axis of the polar C=O bonds and the geometric long axis of these compounds are about perpendicular to each other. Also, in view of the role played by the dione moiety in the transitions $G \rightarrow 2$ and $G \rightarrow 3$ of **3** and **4**, it seems to us dangerous to try to deduce the absolute polarization of these transitions from known data[16] on the parent hydrocarbon acenaphthylene.

5. Conclusions

The MCD spectra combined with appropriately parametrized and adapted semiempirical calculations provide an analysis of the low-lying excited electronic states of the compounds **1–4**. One is able by MCD to resolve some of the unstructured absorption bands and to deduce the symmetry of the transitions involved. Our attempt to complement and confirm our assignments by linear dichroism with use of the stretched-foil technique has, however, been inconclusive. The use of electrochromism for the same purpose might also be difficult.

As the calculations show, the interaction between the dione moiety and the rest of the pseudoaromatic or antiaromatic π-electron system leads to noteworthy charge-transfer effects. One particular aspect is the predicted reversal of the direction of the dipole moment in the excited state 2 of compound **1** and in the excited state 3 of compound **2**.

Another outstanding aspect of compound **2** is the structure of the first, low-lying excited state. The singlet transition $S_0 \rightarrow S_1(^1\pi\pi^*)$ is only very weakly electric dipole allowed. On the other hand, we believe to have detected the A-term of the $S_0 \rightarrow T_1(^3\pi\pi^*)$ transition which arises through spin-orbit coupling. The $S_0 \rightarrow S_1$ transition is mainly centered inside the eight-membered ring and may be interpreted in terms of the perturbed symmetry of the eight-membered cyclic polyene. In our PPP calculations we have for simplicity assumed the molecule to be planar. The MNDO calculations, however, predict it to be of chair form with the terminal carbon atoms on the $(-y)$-side at -0.07 Å below and on the $(+y)$-side at $+0.19$ Å above the yz-plane (see Figure 2). Such nonplanarity which reduces the molecular symmetry from C_{2v} to C_s may possibly enhance the spin-orbit coupling because of the π–σ mixing.

A-terms for $S_0 \rightarrow T_1$ ($^3n\pi^*$) transitions have previously been reported by Dekkers in thioketones[17] and by Meier and one of the present authors in quinones in I. Compound **2** presents to our knowledge the first $S_0 \rightarrow T_1(^3\pi\pi^*)$ transition detected by MCD. The strong spin-orbit coupling in thioketones[17] is obviously due to the sulfur atom. In quinones no substituent-induced heavy-atom effect was observed for the $S_0 \rightarrow T_1(^3n\pi^*)$ transitions (see I), in accord with theoretical predictions.[18] $S_0 \rightarrow T_1(^3\pi\pi^*)$ transitions, on the other hand, are expected to be sensitive to external heavy-atom effects. This has indeed been found in the present case and supports our assignment.

In both compounds **3** and **4** the PPP model interprets the double-signed signal at 350 nm as a pseudo-A-term. In compounds **1–4** the calculations fail to furnish satisfactory descriptions of the shorter wavelength part of the MCD spectra. Because of the increasing density of states it is difficult to pinpoint the dominant contributions to the B-terms.

In general, the PPP calculations give correct orders of magnitude for the quantity B but nevertheless tend to overestimate absolute values. One may also raise the question if the PPP model, because of the restricted AO basis and unpolarizable σ-core, is really suited to predict high-lying $\pi\pi^*$ states. In spite of these limitations the model is still an indispensable help in interpreting the MCD spectra of substituted π-electron systems.

Acknowledgment. This research has in part been supported by the Swiss National Science Fondation. The emission spectrum was measured at the Institute of Biochemistry of the University of Zurich.

(16) Michl, J.; Thulstrup, E. W. Spectroscopy with Polarized Light; VCH Publishers, Inc.: 1986; Chapters 3 and 8.

(17) Dekkers, H. P. J. M. Doctoral Thesis, University of Leiden, The Netherlands, 1975.

(18) El-Sayed, M. A. *J. Chem. Phys.* **1964**, *41*, 2462.